

Grain boundary characteristics of Fe-based superconductors

Kazumasa Iida,^{1,2, a)} Jens Hänisch,³ and Akiyasu Yamamoto^{4, 2}

¹⁾*Department of Materials Physics, Nagoya University, Furo-cho, Chikusa-ku, Nagoya 464-8603, Japan*

²⁾*JST CREST, Sanbancho 5, Chiyoda-ku, Tokyo 102-0075, Japan*

³⁾*Institute for Technical Physics, Karlsruhe Institute of Technology, Hermann-von-Helmholtz-Platz 1, 76344 Eggenstein-Leopoldshafen, Germany*

⁴⁾*Department of Applied Physics, Tokyo University of Agriculture and Technology, 2-24-16 Naka-cho, Koganei-shi, Tokyo 184-8588, Japan*

(Dated: 5 March 2022)

Understanding the nature of grain boundary (GB) characteristics in combination with creating low-energy GBs by modifying the processing conditions, so-called GB engineering, is of great importance for controlling and reducing the defect density, leading to improved functionalities of polycrystalline metals and ceramics. For superconductors particularly, including both low- and high-temperature superconductors, GB engineering has been developed to improve especially the critical current densities, J_c , across these GBs. The intrinsic physical properties of a given superconductor such as the coherence length, the order parameter symmetry, and their anisotropies would determine the strategy of GB engineering. In this topical review, we present an overview of the GB characteristics and GB engineering of Fe-based superconductors (FBS) in the form of polycrystalline bulks and wires, and thin films with application potential, e.g. for high-field magnet wires. Prior to the FBS, GB engineering of the cuprates and MgB_2 are also briefly covered.

^{a)}Electronic mail: iida@mp.pse.nagoya-u.ac.jp

I. INTRODUCTION

Boundaries between adjacent crystallites of typically differing orientation and/or composition are called *grain boundaries*, where the atomic arrangement is in disorder. A grain boundary (GB) with a high interfacial energy (i.e. usually two adjacent grains having a large misorientation angle) is often the origin of macroscopic defects such as cracks and erosion damage, and these defects propagate along the GBs. On the other hand, GBs with a low interfacial energy [e.g. low-angle GBs and coincidence boundaries like twin boundaries] are hardly the origin of macroscopic defects. In low-angle GBs, dense dislocation arrays are formed with a spacing D given by Frank's formula:

$$D = \left(\frac{b}{2}\right) / \sin\left(\frac{\theta_{\text{GB}}}{2}\right) \sim \frac{b}{\theta_{\text{GB}}} \quad (1)$$

where $b = |\vec{b}|$ is the norm of the Burgers vector (for symmetric [001]-tilt GBs in bicrystal films of e.g. cuprates and pnictides as discussed in this review, $|\vec{b}|$ is the in-plane lattice parameter) and θ_{GB} is the misorientation angle between the two adjacent grains.

For both low- and high-temperature superconductors (LTS and HTS), GBs affect their properties: For instance, macroscopic defects (cracks) impede the supercurrent flow. In this case, GBs are detrimental defects to the critical current density J_c and, hence, should be avoided.

For cuprates, not only macroscopic but also microscopic defects are problematic due to the short coherence length ξ (less than 2 nm for ab -plane)¹ and the anisotropic superconducting order parameter (d -wave)². If the strained regions around the dislocations within the GB touch each other, the low-angle GB turns into a high-angle GB. This angle is around $10^\circ \sim 15^\circ$. However, in cuprates a wider region around the centre of the dislocation is perturbed electronically and the inter-grain J_c starts to decrease exponentially already for $\theta_{\text{GB}} < 10^\circ$. Also when

the distance between strained regions is smaller or only slightly larger than the value of ξ within the GB plane, the superconducting order parameter is depressed at the GB and, hence, the super-current flow is impeded. Additionally, bending of the electronic bands at GBs deplete the charge carrier density³, which seriously decreases the superconducting transition temperature T_c . Hence, to achieve large J_c for cuprates, the crystallites should not only be aligned out-of-plane because J_c is anisotropic but also be aligned in-plane within the misorientation angle θ_{GB} , where the distance between strained regions is larger than ξ_{ab} (ξ_{ab} : in-plane coherence length) is satisfied. On the other hand, for LTS and MgB_2 with large coherence length (e.g. 5~6 nm) and s -wave symmetry (for MgB_2 anisotropic s -wave), GBs are able to pin vortices in the mixed state, and especially also GBs with rather large angles. Therefore, increasing the GB densities by reducing the grain size usually leads to improved in-field J_c properties.

As stated above, the symmetry of superconducting order parameter and the coherence length mainly govern the J_c characteristics at GBs for a given superconductor. Hence, for both LTS and HTS, understanding the nature of GB characteristics in combination with modifying the processing conditions, so-called GB engineering, is of great importance for reducing and/or controlling the defect density to tune the superconducting properties.

The Fe-based superconductors (FBS) have similar physical properties as the cuprates, for instance a short coherence length due to the small carrier concentration and a low Fermi velocity⁴. Hence, FBS also seem to share the same GB issues as the cuprates. However, J_c across GBs in FBS is not as severely reduced due to several features, which is reviewed in this article. Many reviews of the synthesis of FBS in the form of bulk samples and thin films, and of their physical properties have been published to date. Additionally, excellent review articles concerning bicrystals and GBs in cuprates have already been published^{3,5,6}, however, only a few on GB issues for FBS have been published (e.g. 7 and 8).

In the following sections, we present an overview of the GB characteristics and GB engineering of the FBS in the form of polycrystalline bulks and wires as well as thin films with application potential, e.g. for high-field magnet wires and compact bulks. In section II, GB engineering of cuprates will be briefly summarised on the basis of the GB characteristics. Section III will describe how GBs affect the superconducting properties of MgB_2 . These sections II and III are relevant for understanding GB issues of FBS. Section IV will present the experimental reports on the misorientation angle dependence of the inter-grain J_c for various FBS films grown on symmetric [001]-tilt bicrystal substrates. In section V, GB engineering of FBS will be presented in the forms of both thin films and polycrystalline samples. The former part will describe how small misorientation angles affect the transport J_c of various FBS films deposited on technical substrates used for the second-generation coated conductors. The latter will present how to improve the superconducting properties of polycrystalline bulk and wire samples. Finally, we will discuss which kind of experiments are desired for better understanding the GB characteristics and summarise the review.

II. GRAIN BOUNDARY ENGINEERING OF CUPRATES

Thanks to T_c values higher than the boiling point of liquid nitrogen, the discovery of cuprates gave a significant excitement on our community. However, some material scientists were pessimistic about cuprates, since polycrystalline $REBa_2Cu_3O_7$ (RE : rare earth elements, $REBCO$) was able to carry only $\sim 100 \text{ A/cm}^2$ even at 4.2 K ⁹, which is far below the level needed for applications. A fundamental problem is that GBs with misorientation angle greater than 3° (this angle is called the critical angle, θ_c) constitute weak links. Figure 1 exemplifies the misorientation angle dependence of J_c for YBCO and Ag-doped YBCO grown on [001]-tilt symmetric SrTiO_3 bicrystal substrates¹⁰. Above θ_c , the angle

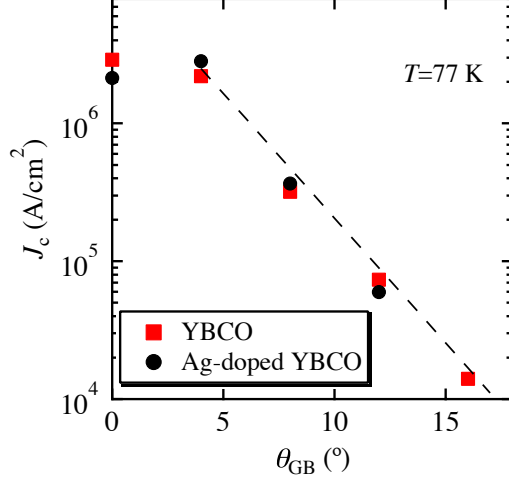


FIG. 1. Critical current density at 77 K of undoped and Ag-doped $\text{YBa}_2\text{Cu}_3\text{O}_7$ (YBCO) films grown on SrTiO_3 [001]-tilt bicrystals of different misorientations. The data are taken from 10. The dashed line is a fit by eq. (2).

dependence of inter-grain J_c (J_c^{GB}) is empirically described by

$$J_c^{\text{GB}}(\theta_{\text{GB}}) = J_c^{\text{G}} \exp\left(-\frac{\theta_{\text{GB}} - \theta_c}{\theta_0}\right) \quad (2)$$

where J_c^{G} is the intra-grain critical current density and θ_0 is the characteristic angle¹⁰. The data were well described by the equation above with $\theta_c=4^\circ$ and $\theta_0=2.4^\circ$. Also for other cuprates (e.g. $\text{Nd}_{1.85}\text{Ce}_{0.15}\text{CuO}_{4-y}$ ¹¹ and $\text{Bi}_2\text{Sr}_2\text{Ca}_2\text{Cu}_3\text{O}_{10+\delta}$ ¹²) inter-grain J_c decreases exponentially with misorientation angle.

Local strain¹³⁻¹⁵ and bending of the electronic band structure¹⁶ resulting from the low carrier density combined with the large dielectric constant reduce the charge carrier density around GBs. As a result, dislocations or whole GB planes

turn into antiferromagnetic insulators (i.e. Mott insulator).

Several models for the microscopic understanding of the transport properties across the GBs for YBCO have been proposed to date. Gurevich and Pashitskii concluded that the misorientation-angle dependence of inter-grain J_c is mainly determined by the progressive decrease in the cross-sectional area of superconductivity, which is induced by local strain¹³. They calculated the critical angle θ_c to be around $3^\circ - 5^\circ$ at 77 K, which is in good agreement with the experimental data. The progressive decrease in superconductivity around GBs is due to the shift of the Fermi level. The Fermi level of the GB regions having a thickness of the order of the Thomas-Fermi screening length lifts up around 5–10 meV due to an excess of ion charge. Such small shifts are strong enough for a phase transition from superconductivity to antiferromagnetism to occur. This model explained the misorientation-angle dependence of inter-grain J_c for the low-angle regime. However, the regions of enhanced strain and possible off-stoichiometries of adjacent dislocations touch and overlap for misorientation angles larger than $\sim 10^\circ$ and, hence, the model cannot be applied for this angular regime. It is worth mentioning that the symmetry of the superconducting order parameter (isotropic s - and anisotropic d -wave) seems not to affect the angle dependence of J_c near the critical angle.

Another calculation based on the bond contraction model showed that the pairing is weakened by the tensile strain surrounding edge dislocations¹⁵. This explains the exponential decay of inter-grain J_c . Kasatkin *et al.* calculated the inter-grain J_c for [001]-tilt GBs on the assumption of the periodic pinning potential along the GBs¹⁷. They calculated the inter-grain J_c as a function of the in-plane coherence length and the norm of the Burgers vector, b , (as stated before, this value corresponds to the in-plane lattice parameter). In this model, the critical angle increases for decreasing ratio of ξ_{ab}/b . The results agree well with the experimental data for YBCO bicrystals with low misorientation angles. However, as pointed out

by the authors, this model cannot explain the larger critical angle of FBS.

For arbitrary misorientation-angles, the inter-grain J_c has been calculated by Graser *et al*¹⁸. They initially simulated the atomic arrangement of YBCO at grain boundaries using a molecular dynamics procedure. Then a tight-binding model including the $d_{x^2-y^2}$ wave symmetry with parameters based on the atomic arrangement determined before was constructed for calculation. This calculation showed also good agreement with the experimental results.

As stated above, GB regions turn into insulating layers, which cannot be explained by the $d_{x^2-y^2}$ wave symmetry of the order parameter alone as pointed out by Schmehl *et al*¹⁹. The product of the grain-boundary normal state resistance R_n and the grain boundary area A is in the range $10^{-9} \leq R_n A \leq 10^{-8} \Omega \text{cm}^2$ at 4.2 K for cuprates²⁰, which is one or two orders of magnitude higher than for Fe-based superconductors. To overcome these problems, Schmehl *et al.* tried to increase the charge carrier density by partially substituting Y^{+3} with Ca^{+2} in YBCO¹⁹. As a result, the inter-grain J_c for [001]-tilt $\text{Y}_{0.7}\text{Ca}_{0.3}\text{Ba}_2\text{Cu}_3\text{O}_{7-\delta}$ bicrystal films with $\theta_{\text{GB}}=24^\circ$ was enhanced by a factor of around 8 at 4.2 K compared to non-doped YBCO. Indeed, $E(J)$ curves at the same reduced temperature ($t=T/T_c=0.85$) for Ca-doped YBCO fabricated on [001]-tilt bicrystal substrate with $\theta_{\text{GB}}=5^\circ$ did not show the non-ohmic linear differential behavior (i.e. the region where electric field E increases linearly with the current density J) known from pure YBCO²¹. Non-ohmic linear differential behavior is caused by viscous flux flow along the grain boundaries²² and hence a clear indication that J_c is limited by GBs. Although Ca-doping mitigates the reduction of inter-grain J_c , the superconducting transition temperature is decreased to the range of $68 \leq T_c \leq 79$ K, when Ca is doped not only in the GB region but also in the adjacent grains. In order to dope Ca only locally whilst grains are kept high- T_c , Hammerl *et al.* fabricated a heterostructure of YBCO/ $\text{Y}_{1-x}\text{Ca}_x\text{Ba}_2\text{Cu}_3\text{O}_{7-\delta}$ on 24° [001]-tilt SrTiO_3 bicrystal²³. As a result, Ca preferentially diffused in the GB region and thereby doped the sample locally

at the GB. The resultant films showed a self-field J_c as high as 3.3×10^5 A/cm² at 77 K, which is almost the same level as for 7° bicrystal films.

Another possible method of increasing the carrier concentration around GBs has been attempted recently by Fâte and Senatore by employing YBCO-based ionic-liquid gate transistors on 8° [001]-tilt SrTiO₃ bicrystal substrates²⁴. Such an electric double layer transistor is a powerful tool to inject a large carrier density of $\sim 8 \times 10^{14}$ cm⁻² at the material's surface²⁵. The authors concluded that the level of carrier density by electrostatic doping was comparable to that of Ca-doping mentioned above. A similar attempt on tuning GB properties by an electric double layer transistor device has been reported by Hassan and Wimbush on La_{1.85}Sr_{0.15}CuO₄ by investigating the resistive transition²⁶.

Another kind of GB engineering is the elimination of high-angle GBs. For this purpose, Jin *et al.* invented a melt-process for YBCO wires²⁷. The resultant sample had a density of 6.2 g/cm³, which is 98% of the theoretical density of YBCO. The self-field J_c of this melt-processed YBCO was almost doubled compared to sintered samples, however, J_c was decreased sharply by small magnetic fields of a few hundred gauss since high-angle GBs were not removed completely.

To eliminate high-angle GBs or at least minimise their density in REBCO bulk superconductors, the top-seeded-melt-growth process has been developed to grow quasi-single crystals²⁸, which means that they contain secondary phase particles within the superconducting matrix and, therefore, are not true single crystals. REBCO bulks can trap large magnetic flux densities, and this ability is determined by $M = NJ_c r$, where M is the volume magnetization, N is a geometrical constant, and r is the diameter of the circulating supercurrent. Hence, a general processing aim in the fabrication of bulk REBCO is the production of large-grain, weak-link-free samples with high J_c . To date, the largest trapped field of 17.6 T in bulk was recorded at 26 K in a stack of two GdBCO bulks with 25 mm in diameter²⁹ (Stacks of high- T_c tape showed a similarly high trapped field of 17.7 T at 8 K³⁰).

Now several companies have commercialised *REBCO* bulk superconductors. Applications by employing *REBCO* bulk superconductors are well summarised in ref. 31.

Similar to *REBCO* bulks fabricated by the top-seeded melt growth process, epitaxial thin films on single-crystal substrates do not contain high-angle grain boundaries. Additionally, growth-related defects such as screw dislocations³² and stacking faults that work as strong pinning centers result in high J_c values of more than 1 MA/cm² at 77 K. However, the question arose how to fabricate single-crystal-like *REBCO* films in long lengths, since a powder-in-tube method is not applicable to fabricating *REBCO* wires. This issue was solved by the development of technical substrates that have been used for the 2nd generation HTS wires, the *REBCO* coated conductors. To date, mainly two kinds of technical substrates have been developed. One is the preparation of textured templates on Hastelloy C-276 tapes by ion beam assisted deposition (IBAD)³³. IBAD yields biaxially textured buffer layers for epitaxial growth of *REBCO*. The other is depositing epitaxial buffer layers on textured NiW tapes, which are thermo-mechanically treated (rolling-assisted biaxial texture, RABiTS)³⁴. Thanks to the recent development of texture quality of those templates, the mean grain mis-orientation of *REBCO* lies in the range of 3–5°. Now tapes with high critical currents I_c and high uniformity of ~ 1 km length are being fabricated, and several companies have commercialised *REBCO* coated conductors. Table I summarises GB engineering for *REBCO* in various forms. As stated above, all methods are based on physical properties of *REBCO*. Hence, it is important to reveal the intrinsic physical properties of superconductors to determine the strategy for tackling GB issues.

TABLE I. GB engineering for *REBCO* in various forms.

Materials form	Methods	Refs.
Bulks	Employing melt-process, top-seeded-melt-growth	27 and 28
Thin films	Ca-doping, electrostatic carrier doping	19, 21, 23, and 24
Tapes	Employing textured templates	33 and 34

III. GRAIN BOUNDARY ENGINEERING OF MgB_2

MgB_2 is a simple binary, metallic superconductor expected to be used at intermediate temperatures. Albeit MgB_2 has a rather high T_c of 39 K and electromagnetic anisotropy of 2-5³⁵, GBs do not show the weak-link limitation of transport current³⁶ due to the large coherence length and anisotropic *s*-wave order parameter symmetry. Soon after the discovery of superconductivity in MgB_2 , high J_c was reported in untextured, polycrystalline wires produced by a powder-in-tube (PIT) process³⁷⁻⁴⁰ owing to its transparent GBs. Like in other intermetallic compound superconductors, GBs belong to the predominant flux pinning centers in MgB_2 ⁴¹⁻⁴⁵. As shown in fig. 2, a strong correlation between J_c and inverse grain size was observed⁴². Therefore, increasing the area density of GBs is an effective strategy to improve J_c . On the other hand, GBs in MgB_2 can be easily covered with impurity phases, such as MgO and amorphous oxides. These insulating particles and/or wetting layers at GBs act as transport current limiters and reduce the connectivity, which deteriorates the inter-grain J_c significantly. In this section, recent activities on GB engineering of MgB_2 bulk samples, namely, controlling GB structure by doping/processing and enhancing GB density by grain size refinement and densification, are briefly introduced.

Refinement of MgB_2 grains has been extensively studied with various methods, including the use of fine boron powder⁴⁶, mechanical refinement by milling⁴⁷⁻⁵⁰, low-temperature heat processing⁵¹⁻⁵⁵, and impurity doping with Ni⁵⁶, Cu⁵⁷⁻⁶⁰, Ag^{61,62}, In⁶³, and Hf⁶⁴. Ma *et al.* reported that lamellar MgB_2 grains can be

formed with Mg–Cu liquid, and these lamellar MgB₂ grains are much better connected than the MgB₂ grains of typical morphology⁶⁰.

Another strategy for increasing the GB density per unit volume is densification, which also contributes to an improvement in connectivity by decreasing porosities. As densification techniques for bulk materials, high pressure synthesis and the magnesium diffusion method are commonly employed. To date, disk-shaped MgB₂ bulks prepared by a hot-pressing technique have been prepared by many groups^{65–68}, and the resultant trapped field reached 3 T⁶⁵. Nearly fully dense MgB₂ bulks can be obtained by spark plasma sintering in a relatively short time (less than an hour)^{69–74}. The magnesium diffusion/infiltration technique is known

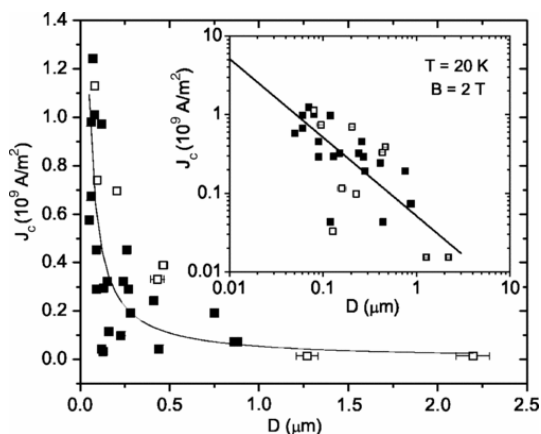


FIG. 2. Grain size (D) dependence of J_c for dense MgB₂ samples. The line fits to the $1/D$ dependence. The open symbols are non-doped samples and the solid symbols are doped samples. Reprinted with permission from 42. Copyright (2017) by the American Physical Society.

as an alternative way to obtain dense MgB₂ wires/bulks without applying high pressure during heating⁷⁵⁻⁷⁹. Bhagurkar *et al.* reported nearly fully dense undoped and carbon-doped MgB₂ bulks fabricated by the infiltration and growth process⁸⁰⁻⁸². High trapped fields of ~ 3 T have been measured at 5 K at the center of a stack of two bulk MgB₂ samples fabricated using this technique⁸⁰. Owing to the progress in the technologies of producing relatively large, dense MgB₂ bulks, efforts in new bulk application fields, including magnetic shielding⁸³, magnetic levitation⁸⁴, and biomedical applications³¹, as well as permanent-magnet applications have begun.

IV. θ_{GB} DEPENDENCE OF INTER-GRAIN J_c FOR FE-BASED SUPERCONDUCTING BICRYSTAL FILMS

A. NdFeAs(O,F)

In the early stage of FBS research, LaFeAs(O,F)^{85,86}, SmFeAsO_{0.85}, NdFeAs(O,F)⁸⁷, and SmFeAs(O,F)⁸⁸ exhibited electromagnetic granularity similar to the cuprates. On the other hand, clear Meissner state due to bulk diamagnetism was observed in polycrystalline bulk $Ln\text{FeAs}(\text{O},\text{F})$ (Ln : lanthanoide) samples by magneto-optical imaging at a magnetic field below the lower critical field H_{c1} ⁸⁹. Moreover, the roof top pattern was observed in the remanent magnetic field distribution image of the field-cooled sample, suggesting the macroscopic critical state of the whole bulk. Although J_c was higher than that of the untextured cuprates, it was still one or two orders of magnitude lower than MgB₂, which does not show weak-link behaviour. Detailed microstructural analysis revealed that the early polycrystalline samples were multiphase composites containing impurities and structural defects, such as cracks and an amorphous wetting phase⁸⁷. GBs of these samples were random and mixed with tilt and twist grain boundaries. Additionally, clean grain boundaries (i.e. no impurities between the grains) were

also confirmed. To understand the effect of intrinsic and extrinsic factors on GB transport properties, bicrystal experiments on $LnFeAs(O,F)$ with single GB have been long desired. Under such circumstances, Omura *et al.* grew $NdFeAs(O,F)$ films on MgO bicrystal substrates with [001]-tilt GB of various misorientation angles by molecular beam epitaxy⁹⁰. Here, $NdFeAs(O,F)$ thin films have been fabricated via a two-step process: Parent $NdFeAsO$ is fabricated and subsequently a $NdOF$ overlayer is deposited on $NdFeAsO$ for F-doping⁹¹. Figure 3 shows the misorientation angle dependence of the GB transparency J_c^{GB}/J_c^G (J_c^{GB} : inter-grain J_c , J_c^G : intra-grain J_c) for $NdFeAs(O,F)$ fabricated on symmetric [001]-tilt MgO bicrystal substrates measured at 4.2 K. The inter-grain J_c was reduced by 30% compared to the intra-grain J_c even at $\theta_{GB}=6^\circ$, indicating that the critical angle for those samples may be less than 6° . However, the results show an extrinsic effect because $NdFeAs(O,F)$ was damaged by excess F. The $NdOF/NdFeAs(O,F)$ bilayer is similar to $Y_{0.7}Ca_{0.3}Ba_2Cu_3O_{7-\delta}/YBCO$. As known from the work of $Y_{0.7}Ca_{0.3}Ba_2Cu_3O_{7-\delta}/YBCO$ bilayer²³, Ca preferentially diffused through the GB and enriched Ca around the YBCO grains. Similarly, F diffused along the GB in $NdFeAs(O,F)$, however, the excess F deteriorated the $NdFeAs(O,F)$ layers due to the strong reactivity. To extract the intrinsic nature of the GBs in $NdFeAs(O,F)$, the damage around the GBs had to be minimised. Hence, the $NdOF$ overlayer was deposited at $750^\circ C$ instead of $800^\circ C$ in order to suppress the excess F diffusion along the GB. With this method J_c^{GB}/J_c^G is at nearly constant value of unity up to 8.5° (Figure 3)⁹². Beyond 8.5° , J_c^{GB}/J_c^G decreases with θ_{GB} . Another distinct feature is that J_c^{GB}/J_c^G is larger than 1 at $\theta_{GB}=6^\circ$. A plausible reason for this phenomenon is GB pinning. This may explain the improvement of J_c for Co- and P-doped $BaFe_2As_2$ deposited on technical substrates^{93,94}, which is discussed later.

Lowering the deposition temperature for the $NdOF$ overlayer certainly improved the GB properties of $NdFeAs(O,F)$. However, both inter- and intra-grain J_c in self-field was of the order of 10^5 A/cm²⁹², which is one order of magnitude lower than

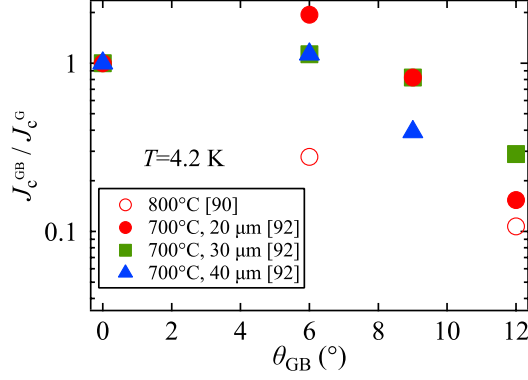


FIG. 3. Angle dependence of the GB transparency J_c^{GB}/J_c^G at 4.2 K for NdFeAs(O,F) bicrystal films with different deposition temperatures and thicknesses of the NdOF overlayer.

that of an ordinary NdFeAs(O,F) (i.e. deposition temperature of NdOF is 800°C). Additionally, damage to the GB region by F is inevitable despite lowering the deposition temperature of NdOF. Therefore, studying F-free oxypnictide would be necessary. To date, polycrystalline $Ln(\text{Fe},\text{Co})\text{AsO}$ ⁹⁵ and epitaxial $\text{SmFeAs}(\text{O},\text{H})$ ⁹⁶ thin films are available and, therefore, studying the GB angle dependence of J_c of bicrystal films of those compounds would be reasonable.

B. Co- and P-doped BaFe_2As_2

Lee *et al.* in 2009 were the first to show possible weak-link behaviour of [001]-tilt GBs in $\text{Ba}(\text{Fe}_{1-x}\text{Co}_x)_2\text{As}_2$ films ($T_c=20.5$ K) grown by pulsed laser deposition on

bicrystalline SrTiO₃ substrates containing GBs with angles θ_{GB} of 3°, 6°, 9°, and 24°⁹⁷. Also the low-angle GBs with $\theta_{\text{GB}}=6^\circ$ and 9° showed weak-link behaviour in low-temperature laser scanning microscopy and magneto-optical imaging. This suggested a critical angle $\theta_c < 6^\circ$, which later turned out to be in contrast to the results reported by Katase, Hiramatsu *et al.*^{98,99} with a critical angle $\theta_c \sim 9^\circ$ from Ba(Fe_{1-x}Co_x)₂As₂ films on MgO ($T_c=20.7$ K) and LSAT ($T_c=21.6$ K) bicrystals. Presumably, an increased oxygen diffusion from SrTiO₃ under ultra high vacuum conditions along the GB leads to a slightly broader region of reduced order parameter around the GB which may have caused the J_c reduction of the low-angle

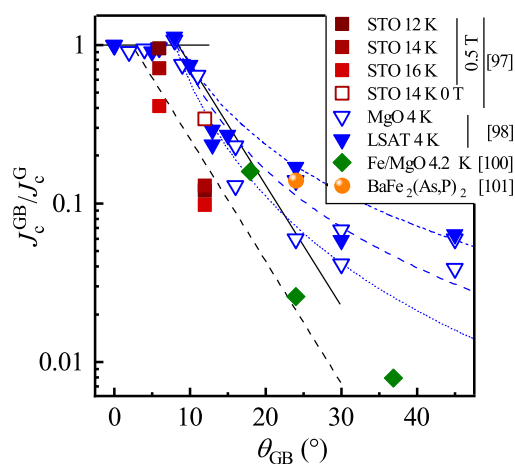


FIG. 4. Angle dependence of the GB transparency for Ba(Fe_{1-x}Co_x)₂As₂ bicrystal films on different substrates [(LaAlO₃)_{0.3}(Sr₂TaAlO₆)_{0.7} (LSAT), SrTiO₃ (STO) and Fe-buffered MgO (Fe/MgO)] grown by pulsed laser deposition and a BaFe₂(As_{1-x}P_x)₂ bicrystal film on MgO grown by molecular beam epitaxy. The lines are exponential (black) and power-law (blue) approximations of the data according to eqs. 2 and 3, respectively.

GB⁹⁷. T_c was only minimally reduced across the 6° junction on SrTiO₃ by 0.2 K with sharp resistive transition. Nevertheless, the elevated applied fields (500 mT) and measurement temperatures (12, 14 and 16 K) in⁹⁷ should be regarded (data at low temperature and magnetic field are comparable to the ones reported in^{98,99}, fig. 4). Later, Iida *et al.* investigated high-angle GBs in Ba(Fe_{1-x}Co_x)₂As₂ films grown on Fe/spinel-buffered SrTiO₃ bicrystal substrates¹⁰⁰. The critical angle was around 8°. The J_c reduction of the high-angle GBs, nevertheless, was 10 times larger than shown by Katase *et al.*, which again is most likely due to defects in the GB region because of the oxygen diffusion from SrTiO₃. Sakagami *et al.* showed J_c^{GB} as high as 1 MA/cm² at 4 K for $\theta_{\text{GB}}=24^\circ$ for a BaFe₂(As_{1-x}P_x)₂ film on an MgO bicrystal grown by molecular beam epitaxy¹⁰¹, which is due to the higher T_c and hence higher J_c^{G} than for Co-doped BaFe₂As₂. Despite the low number of data points, θ_c of BaFe₂(As_{1-x}P_x)₂ is most likely also larger than for the cuprates. The $J_c(\theta_{\text{GB}})$ dependence for GBs in Co- and P-doped BaFe₂As₂ as available in literature is summarised in Figure 4. Clearly, J_c^{GB} remains at J_c^{G} up to $\theta_c \sim 9^\circ$. At higher angles, exponential decay of the GB transparency with a slope similar to that of the cuprates (dashed black line) is observed. J_c^{GB} is, on the other hand, nearly constant for 30° and 45°. An alternative possible phenomenological description of the data beyond θ_c is shown as blue dashed lines according to

$$\frac{J_c^{\text{GB}}}{J_c^{\text{G}}} = \left(\frac{\theta_{\text{GB}}}{\theta_0} \right)^{-n} \quad (3)$$

with sets of parameters (θ_0, n) of (8.5, 1.7), (8.25, 2.05), and (8.0, 2.4) for high, medium and low J_c values, respectively. Such a function might be worthwhile for testing in statistical simulation models of GB networks such as in ref.¹⁰², however the differences to the logarithmic fits may be small, especially for sharp textures.

Occasionally, pinning effects can be observed in single high-angle GBs, even though the absolute J_c value might not be higher than the intra-grain values. An example is found in ref.⁹⁷ for the 24° GB junction of Ba(Fe_{1-x}Co_x)₂As₂ on SrTiO₃.

Despite the lower J_c values for all applied fields, a peak effect is visible near 5 T which can be attributed to pinning of vortices in the GB plane or surrounding region itself as well as by interaction with vortices in the grains nearby. In ref. ⁹⁸, this effect can be recognised as well but is not discussed there. High-angle GBs can also supply pinning centres indirectly: Fe nanoparticles preferably grow in or near such GBs, see ref. ¹⁰³, most likely because of higher diffusion rates in the grain boundaries or strain effects. J_c of the sample with these 45° GBs was increased in a wide range of field and temperature compared to a similar sample without 45° misorientations with a pronounced c -axis peak due to the c -axis-oriented GBs and the slightly c -axis-elongated Fe nanoparticles.

C. Fe(Se,Te)

A self-field inter-grain J_c of around 10^4 A/cm² at low temperatures for Fe(Se,Te) of a 45° GB ¹⁰⁴, only 10 times lower than the intra-grain J_c (instead of 10^4 as for the cuprates) suggested a J_c decrease with θ_{GB} not as strong as for the cuprates. J_c values being rather independent of the bridge width and the uniform Josephson current along the junction were attributed by Sarnelli *et al.* to the s -wave symmetry in these materials. Later, the full $J_c(\theta_{\text{GB}})$ dependence with $\theta_c \sim 9^\circ$ was measured by Si *et al.* ¹⁰⁵ and Sarnelli *et al.* ¹⁰⁶, see fig. 5. As Si *et al.* found, $J_c(\theta_{\text{GB}})$ maintains $\sim 10^5$ A/cm² at 4.2 K for $\theta_{\text{GB}} < 7^\circ$ even in applied fields of around 10 T, showing that these GBs are strong links. For $\theta_{\text{GB}} > 15^\circ$ the GBs showed significantly lower J_c values and a foot structure in the temperature dependence of the resistivity, $\rho(T)$, due to a larger distorted region near the GB. If intrinsic effects, such as thermally activated phase slippage ¹⁰⁷, may contribute in such samples with low T_c values, is still to be investigated. In contrast to Nd-FeAs(O,F) and Ba(Fe_{1-x}Co_x)₂As₂, the GB transparency also decreased below θ_c , and no increased values were found near θ_c . However, further experiments in the

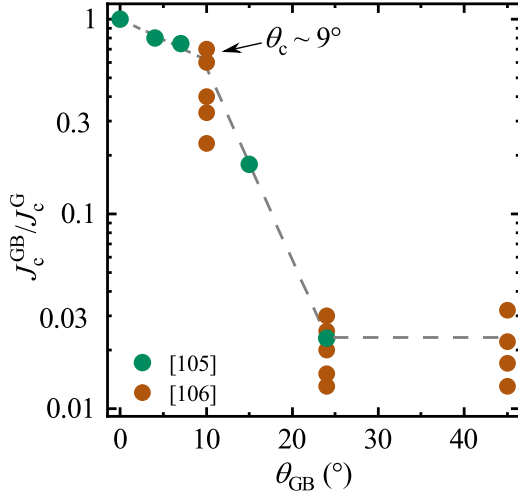


FIG. 5. Angle dependence of the self-field GB transparency for Fe(Se,Te) bicrystal junctions at 4 K.

vicinity of the critical angle are necessary to clarify this. The level of J_c^{GB} is almost constant above 24° ¹⁰⁶.

V. GRAIN BOUNDARY ENGINEERING OF FE-BASED SUPERCONDUCTORS

A. Grain boundary networks in Fe-based superconducting films

Long-length YBCO coated conductors are fabricated on polycrystalline templates, which are in- and out-of-plane textured. Hence, thin films on technical substrates (e.g. Hastelloy) contain many low-angle GBs, which provides a good platform for studying how low-angle GB networks affect J_c . To date, most of

the FBS coated conductors as proof-of-principle studies have been fabricated on metallic templates with biaxially textured MgO prepared by IBAD. Fe(Se,Te) has been also deposited on CeO₂-buffered RABiTS. Here, we briefly review each FBS on technical substrates.

1. *LnFeAs(O,F)*.

So far, only NdFeAs(O,F) has been grown on a technical substrate among *LnFeAs(O,F)*. Iida, Hänisch *et al.* reported on the fabrication of NdFeAs(O,F) on IBAD-MgO by molecular beam epitaxy¹⁰⁸. Structural characterization by X-ray diffraction revealed some 45° rotated grains, resulting in a low self-field J_c at 5 K of 70 kA/cm² (corresponding to a reduced temperature of $t=T/T_{c,0}=0.135$), which is comparable to the 40 kA/cm² at 4.2 K measured for partially textured PIT Sm-FeAs(O,F) tape¹⁰⁹. However, it was 1.5 times lower than J_c on MgO single crystal of 3 MA/cm²¹¹⁰. After optimisation of the deposition conditions for NdFeAs(O,F) on IBAD-MgO, rotated grains were successfully removed, resulting in a record self-field J_c for this kind of films of around 2 MA/cm²¹¹¹.

2. *Ba(Fe_{1-x}Co_x)₂As₂*.

Already in 2011, Ba(Fe_{1-x}Co_x)₂As₂ films were grown on Fe-buffered IBAD-MgO templates by pulsed laser deposition¹¹². The films were biaxially textured, and the crystalline quality of both Fe-buffer and superconducting layers with full width at half maximum values of $\Delta\phi_{\text{Fe}}\sim 5^\circ$ and $\Delta\phi_{\text{Ba122}}\sim 5^\circ$ was comparable to that of the MgO ($\Delta\phi_{\text{MgO}}\sim 6^\circ$). The Ba(Fe_{1-x}Co_x)₂As₂ coated conductor showed an onset T_c of 22 K ($T_{c,0}=17.5$ K), which was a relatively large transition width. Due to the poor crystalline quality, the self-field J_c of 0.1 MA/cm² at 8 K ($t=0.457$) was 8-10 times lower than on single crystalline MgO. This electro-magnetic granularity in Ba(Fe_{1-x}Co_x)₂As₂ coated conductors was later suppressed by employing

a sharply in-plane textured MgO ($\Delta\phi_{\text{MgO}}=2.4^\circ$), leading to a J_c level comparable to the film on single crystalline substrate¹¹³. Shortly after, Katase *et al.* grew $\text{Ba}(\text{Fe}_{1-x}\text{Co}_x)_2\text{As}_2$ on IBAD-MgO without a buffer layer⁹³. Thanks to the self-epitaxy effect, a sharp in-plane texture of $\Delta\phi_{\text{Ba122}}=3.2\text{-}3.5^\circ$ was reached irrespective of the template's $\Delta\phi_{\text{MgO}}$ values.

Although J_c is limited by GBs in general, GBs in FBS also have advantages: a) The larger θ_c than for the cuprates (as reviewed above) allows for less-textured templates. b) GBs may contribute to flux pinning, resulting in high current carrying capabilities in magnetic field⁹³: $\text{Ba}(\text{Fe}_{1-x}\text{Co}_x)_2\text{As}_2$ films on IBAD-MgO of different in-plane full width at half maximum values ($\Delta\phi_{\text{MgO}}=5.5^\circ, 6.1^\circ, 7.3^\circ$) lead to $\text{Ba}(\text{Fe}_{1-x}\text{Co}_x)_2\text{As}_2$ texture spreads of $\Delta\phi_{\text{Ba122}}=3.1^\circ, 3.2^\circ$, and 3.5° . Apparently, the self-field J_c (1.2, 1.6, 3.6 MA/cm²) is correlated to $\Delta\phi_{\text{Ba122}}$, which is due to θ_{GB} of most GBs being below θ_c (i.e. they are strong links) and due to an increasing dislocation density with misorientation spread. One of the films on IBAD-MgO ($\Delta\phi_{\text{MgO}}=6.1^\circ$) showing higher $J_c(B\parallel c)$ values than a film on MgO single crystal for all fields at low and medium temperature and even higher than $J_c(B\parallel ab)$ up to a temperature-dependent cross-over field supported this finding.

Xu *et al.* reported recently on the growth of $\text{Ba}(\text{Fe}_{1-x}\text{Co}_x)_2\text{As}_2$ on SrTiO₃/LaMnO₃-buffered IBAD-MgO¹¹⁴. Almost isotropic J_c of 0.86 and 0.96 MA/cm² at 9 T and for $B\parallel c$ and $B\parallel ab$, respectively, were recorded at 4.2 K.

To understand the J_c - B properties of FBS grown on technical substrates, Abrikosov-Josephson vortices should also be taken into account. Abrikosov vortices with Josephson cores, so-called Abrikosov-Josephson vortices, are present in low-angle GBs for YBCO^{115,116}. Although there are no reports on Abrikosov-Josephson vortices in FBS, they might be present in GB networks having small misorientation angles. As has been reported by Palau *et al.* for cuprates¹¹⁷, the inter-grain J_c correlates with intra-grain J_c due to the magnetic interaction between Abrikosov-Josephson vortices at low-angle GBs and Abrikosov vortices

in the grains. Hence, it is possible to improve the pinning potential of Abrikosov-Josephson vortices by increasing the density of strong pinning centres in close vicinity of the GB region.

3. $BaFe_2(As_{1-x}P_x)_2$.

Sato *et al.* grew $BaFe_2(As_{1-x}P_x)_2$ on IBAD-MgO with $\Delta\phi_{MgO}=4^\circ$ and 8° ⁹⁴ by pulsed laser deposition. Energy dispersive X-ray spectroscopy in TEM cross sectional images showed clean and homogeneous GBs. The grain size of ~ 100 nm as well as dislocation arrays in the GB regions were seen in plane-view TEM images

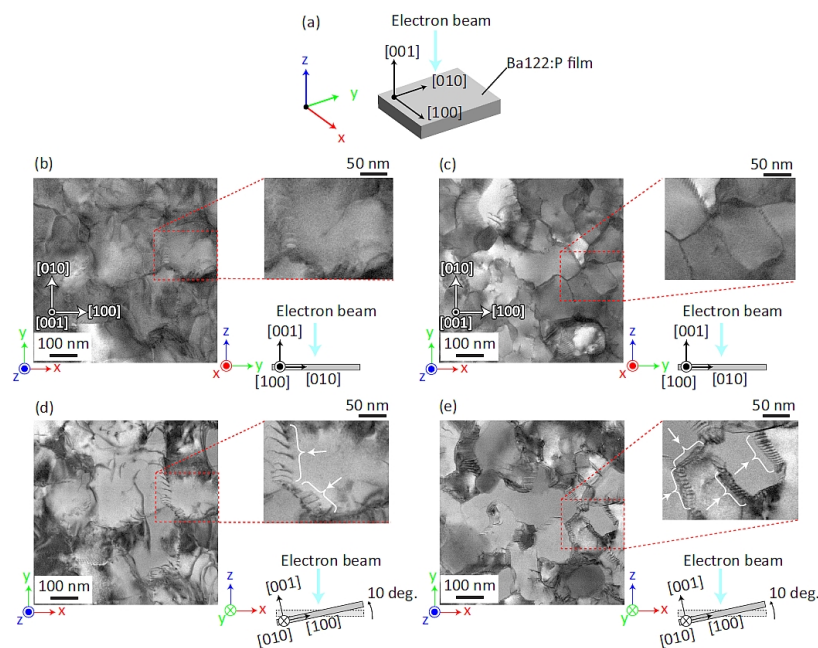


FIG. 6. Plane-view bright-field scanning TEM images of $BaFe_2(As_{1-x}P_x)_2$ films on two IBAD templates with $\Delta\phi_{MgO}=4^\circ$ and 8° . (a) Relationship between film orientation, incident electron beam, and global axes (X, Y, and Z). (b, c) Typical plane-view images by normal electron beam incidence for $\Delta\phi_{MgO}=4^\circ$ (b) and 8° (c). (d, e) Slanted-angle images (tilting by 10°) for visualizing dislocations at same areas of (b, c), respectively. The arrows in the top right image of (d, e) show arrays of dislocations. Reproduced with permission from Sato *et al.*, *Sci. Rep.* **6**, 36828 (2016). Copyright 2016 Springer Nature.

(fig. 6). The crystalline quality of the film on the 4° substrate was better than that of the film on MgO with $\Delta\phi_{\text{MgO}}=8^\circ$, and its $T_{c,0}$ of 23 K was 4 K higher than for the 8° substrate. Nevertheless, the film on the 8° substrate showed a larger c -axis peak and 1.5 times higher J_c values than the 4° template, which is due to the larger density of especially vertical defects related to the GB networks. Since it has a higher J_c and therefore also irreversibility line, the 4° sample surpasses the 8° sample at a temperature-dependent crossover field. However, the 8° sample still shows the stronger c -axis peak. One of these samples on 8° template was further investigated in high fields¹¹⁸. The field-dependent pinning force densities, $F_p(H)$, analysed with the modified Dew-Hughes model, suggest that pinning is strongly dominated by surface pinning, i.e. on 2-dimensional defects in the matrix such as dislocation networks and full GBs. The $V(I)$ curves clearly showed a crossover between GB limitation (non-ohmic linear differential) at low fields and and pinning limitation (power law behaviour, representing flux creep effect) at high fields. Similar non-ohmic linear differential behaviour has been measured for $\text{Ba}(\text{Fe}_{1-x}\text{Co}_x)_2\text{As}_2$ with 45° and (110) misoriented grains¹¹⁹ and polycrystalline $\text{SmFeAsO}_{0.85}$ ¹²⁰.

A first 10 cm long $\text{BaFe}_2(\text{As}_{1-x}\text{P}_x)_2$ tape was fabricated by pulsed laser deposition with a reel-to-reel system at a tape travelling speed of 6 mm/min¹²¹, and its $T_{c,0}$ was reduced ~ 17 K, which is slightly low compared to the static samples ($T_{c,0}\sim 20$ K). I_c was 0.47 mA/cm-width at 4.2 K, corresponding to $J_c=47$ kA/cm². For enhancing T_c and J_c , $\text{Fe}_3\text{P}/\text{BaFe}_2(\text{As}_{1-x}\text{P}_x)_2$ bilayers were fabricated on IBAD-MgO. This led to improved $T_{c,0}$ of 24 K and I_c of 975 mA/cm-width ($J_c=175$ kA/cm²) at 4.2 K.

4. *Fe(Se,Te)*.

Si *et al.* were able to deposit high quality Fe(Se,Te) films on IBAD-MgO despite the relatively large mismatch of 9.5%¹²². The in- and out-of-plane full width at half maximum values of Fe(Se,Te) were $\Delta\phi_{\text{Fe(Se,Te)}}=4.5^\circ$ ($<\theta_c$) and $\Delta\omega_{\text{Fe(Se,Te)}}=3.5^\circ$. Since also [010]-tilt GBs in FBS probably have a similar θ_c value, the GBs do not act as weak-links in these films. The lower $T_{c,0}$ of 11 K compared to single crystalline LaAlO₃ substrate (~ 15 K) can be attributed to the large misfit and reduces self-field J_c at 4 K to 0.2 MA/cm². Xu *et al.* grew Fe(Se,Te) films on LaMnO₃/IBAD-MgO¹²³. The T_c of 15.8 K was slightly enhanced due to the in-plane lattice compression. Whereas $\Delta\omega_{\text{Fe(Se,Te)}}=3.4^\circ$ was similar to the film in ref.¹²², $\Delta\phi_{\text{Fe(Se,Te)}}=7.8^\circ < \theta_c$ was larger. The self-field J_c at 4.2 K was 0.43 MA/cm² nonetheless.

Not only IBAD-MgO templates but also CeO₂-buffered RABiTS were used for the growth of Fe(Se,Te) films¹²⁴. The relevant lattice parameter of CeO₂ is around 3.82 Å, hence close to the in-plane parameters of Fe(Se,Te). Si *et al.* achieved films on RABiTS with a high T_c of ~ 20 K and sharp resistive transition, which may be due to the small lattice mismatch and absence of intercalated Fe. Even though the in-plane full width at half maximum value was $\sim 6^\circ$, (corresponding to the underlying template of $\Delta\phi_{\text{CeO}_2}=7^\circ$), a large self-field J_c of 1.5 MA/cm² at 4.2 K was measured. According to the authors, the CeO₂ buffer layer is more important for the superconducting properties than the texture spread in this system. That means again GBs with angles up to 7° do not obstruct the current flow. To reduce the necessary number of buffer layers, Sylva *et al.* recently deposited Fe(Se,Te) on Ni₅W with a single CeO₂ buffer layer by pulsed laser deposition¹²⁵. This sample showed $T_c \sim 18$ K (due to slight Ni poisoning) and a self-field $J_c \sim 0.1$ MA/cm² as well as $J_c(H) > 20$ kA/cm² up to 18 T at 4.2 K.

B. $AeFe_2As_2$ ($Ae=\text{Sr}$ and Ba) polycrystalline samples

The Ae -122 system is one of the most actively researched FBS for magnet applications owing to its moderately high T_c (38 K for K-doped Ba-122), high B_{c2} (above 50 T) and small electromagnetic anisotropy^{126,127}. In recent years, high- J_c wires^{128–130}, pancake coil tests¹³¹, and demonstration of bulk magnet trapping over 1 T^{132–134} have been reported. The synthesis and GB engineering guidelines for the Ae -122 system fall into two different categories: uniaxial texturing of polycrystals, and making randomly oriented polycrystals without texturing. The former and latter guidelines are similar to those for $\text{Bi}_2\text{Sr}_2\text{Ca}_2\text{Cu}_3\text{O}_{10+\delta}$ tapes and MgB_2 , respectively. For tape wires with their flat geometry produced by the PIT method, a uniaxially aligned microstructure can be obtained relatively easily by employing plate-like Ae -122 powder and cold working. On the other hand, for untextured polycrystalline forms such as bulks or round wires, high transport J_c can be successfully achieved by grain boundary engineering, which is discussed below.

High transport J_c in Ag-clad $\text{Sr}_{0.6}\text{K}_{0.4}\text{Fe}_2\text{As}_2$ tapes prepared by the *ex-situ* PIT method was reported by Zhang *et al*¹²⁹. To produce Sr-122 powder, Sr fillings, K pieces, and Fe and As powders were mixed and heat-treated at 900°C for 35 h. In order to improve the grain connectivity, 5wt% Sn was added. After packing the powder into Ag tubes, drawing, flat rolling and hot pressing at 850°C under 30 MPa, Sr-122 tapes with 0.4 mm in thickness were obtained. J_c of the Sr-122 tape was over 10^5 A/cm² in 10 T at 4.2 K, and still remained at 8.4×10^4 A/cm² up to 14 T. The high J_c in the Sr-122 tapes may be attributed to the combination of improved grain connectivity, grain texture, and inherently strong pinning. The c -axis orientation factor for the tape was 0.52, suggesting grain texturing after pressing. Such grain texturing is considered to alleviate weak-link behaviour at GBs and can also be achieved by high pressure sintering^{135–137} and conventional cold mechanical deformation processes^{127,130,138–141}. Ag-based Sn binary alloys were deployed for *ex-situ* Ba-122 tapes as sheath material by Togano *et al*¹⁴². The Ag-Sn alloy has

higher mechanical strength compared to pure Ag. Successful densification and texturing of the Ba-122 core were obtained. The Ag-Sn-sheathed Ba-122 tapes showed higher transport J_c compared to those of Ag-sheathed tapes. The authors further pointed out the significantly improved smoothness of the interface between the sheath and Ba-122 core. These findings indicate the benefit of using high mechanical strength sheath. Surprisingly high J_c values in randomly oriented, fine-grain wires and bulks were reported by Weiss *et al*¹²⁸. Sub-micron size Ba-122 powders were prepared by a mechanochemical reaction¹⁴³. TEM showed that the average grain size is approximately 200 nm. The randomly oriented polycrystalline structure contained many high-angle grain boundaries including clean and well

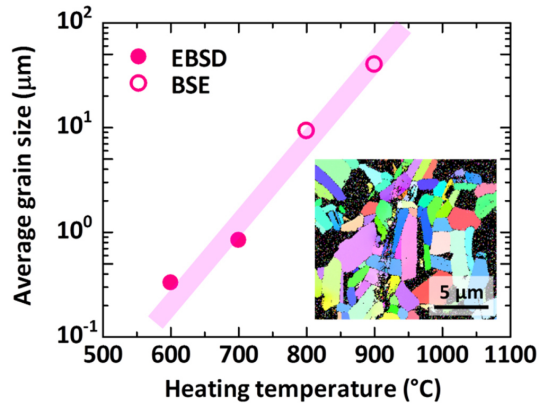


FIG. 7. Clear correlation between average grain size and processing temperature can be seen for polycrystalline Co-doped Ba-122. The inset displays the inverse pole figure map obtained by scanning electron microscope EBSD for a sample heated at 700°C for 48 h. BSE stands for back-scattered electron. Reproduced from 146.

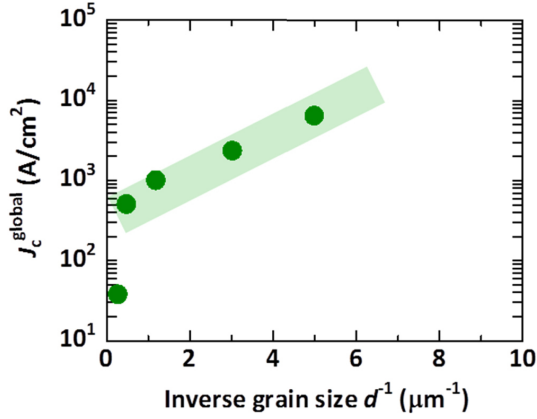


FIG. 8. Inverse grain size ($1/d$) dependence of the global J_c for Co-doped Ba-122 polycrystalline samples. Reproduced from 146.

connected ones. J_c at 4 K reached 1.2×10^5 A/cm² and 2×10^4 A/cm² for Ba-122 wires with K-doping and Co-doping, respectively. Quite recently, the additional effect by ball milling was reported by Tokuta and Yamamoto¹⁴⁴: high-energy ball milling introduces lattice defects in Co-doped Ba-122, resulting in high H_{c2} .

The influence of grain size, especially the benefit of small grains, was studied by Hecher *et al.* based on the Josephson junction network model¹⁴⁵. Scanning Hall probe microscopy and magnetic hysteresis measurements on Ba-122 bulks with systematically varied grain size showed that the field dependence of untextured polycrystalline samples can be significantly reduced when the grain size is small. Shimada *et al.* reported on detailed microstructural investigations of the Ba-122 bulk samples prepared at different heating temperatures¹⁴⁶. A strong heating temperature dependence of the average grain size was observed for the temperature

range between 600°C and 900°C (fig. 7). Interestingly, a relationship between inverse grain size and magnetization J_c was confirmed, as shown in fig. 8, which also supports that a small grain size would be preferable for randomly oriented polycrystalline Ba-122 samples.

Another key issue to address is chemical composition at grain boundaries. Kim *et al.* reported grain and grain boundary composition in K-doped Ba-122 polycrystals by atom-probe tomography¹⁴⁷. Significant compositional variation and segregation of oxygen impurities at grain boundaries were observed. These would suppress transport current across grain boundaries. Detailed microstructural and electromagnetic investigation on artificial grain boundaries in bicrystal and natural grain boundaries in polycrystalline samples are very helpful for grain boundary engineering in this system.

VI. DISCUSSION AND SUMMARY

Artificial, well-defined single grain boundaries have been used for fundamental investigations such as J_c transparency as a function of mis-orientation angle θ_{GB} . For [001]-tilt symmetric bicrystal films, Fe(Se,Te), Co-doped Ba-122 and Nd-FeAs(O,F) showed the same critical angle θ_c of around 9°, which is larger than for cuprates. The dominant factor for governing θ_c may be the symmetry of the order parameter. The reduction of current-carrying cross-section of GB regions by strain effects also controls the θ_c as discussed by Gurevich and Pashitskii.¹³, since the sensitivity of superconductivity by strain is different for FBS and cuprates. Additionally, the local off-stoichiometry near GBs affects the size of the normal core regions¹³. Although θ_c is different for FBS and cuprates, both superconductors showed an exponential decay of inter-grain J_c with nearly the same slope for medium angles. However, for $\theta_{GB} > 24^\circ$ the inter-grain J_c for Co-doped Ba-122 and Fe(Se,Te) is almost constant, whereas such behaviour is absent for cuprates.

Unlike YBCO, the microscopic understanding of GBs is still limited. To understand the GB characteristics, therefore, detailed microstructural analyses should be carried out to map out the local strain around the GBs. To rule out local off-stoichiometry, bicrystal experiments using stoichiometric superconductors (e.g. LiFeAs and FeSe or even $\text{CaKFe}_4\text{As}_4$) would be interesting for further studies.

Another distinct feature is that the product of the grain-boundary normal state resistance R_n and the grain boundary area A for FBS is one or two orders of magnitude lower than that for cuprates due to the metallic nature of GBs (fig. 9). Here, R_n corresponds to the slope of V - I in the non-ohmic linear differential region and A is the cross sectional area of the microbridge for transport measurements. For YBCO, band bending creates charge depletion layers around the GBs, which leads to the formation of insulating layers (Mott insulator)¹⁶. The presence of insulating layers at large-angle GBs was experimentally confirmed by Winkler *et al.* on YBCO bicrystal Josephson junctions¹⁴⁸. For doped FBS, even if the depletion layers are formed at GBs by some mechanisms like strain effects, GB regions stay in the metallic state. This may be a part of the reason why the GBs of FBS are of metallic nature.

The critical angle as well as the θ_{GB} dependence of the inter-grain J_c could be different for other types of bicrystals (i.e. [010]-tilt roof and valley, and twist). Hence, various types of bicrystal experiments should be carried out in order to deeply understand the characteristics of GBs, which is very important for the applications using a polycrystalline form such as PIT wires and bulk magnets.

Regarding applications, bicrystal experiments on K-doped Ba-122, which is believed to be an important material, should be carried out. Experiments on single GBs in polycrystalline K-doped Ba-122 films have been reported¹⁴⁹. However, the information on well-defined, single GBs is necessary for deep understanding of GB characteristics. Due to the difficulty of the thin film growth, no studies on epitaxial K-doped Ba-122 thin films have been reported to date. Very recently, we

have successfully fabricated epitaxial K-doped Ba-122¹⁵⁰, which opens an avenue for such bicrystal experiments.

Clean GBs without wetting phase may not become obstacles for inter-grain super-currents irrespective of the mis-orientation angle, which is similar to MgB₂. Even a high GB density acts as pinning centre ensemble.

From the above, grain boundary properties of FBS may be also located in between MgB₂ and cuprates. Nevertheless, fundamental understanding of GB properties leads to further improvement of the current carrying capability of FBS by GB engineering.

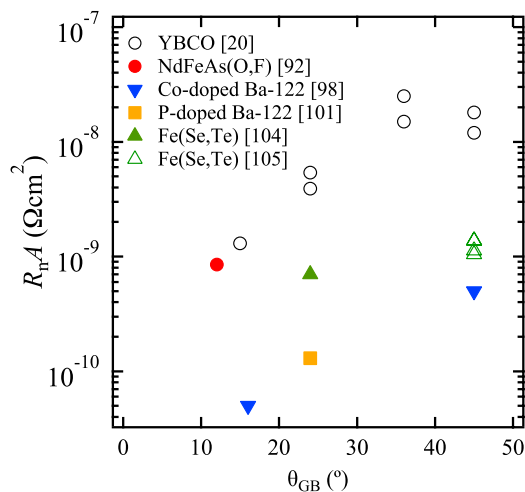


FIG. 9. Comparative θ_{GB} dependence of resistance area product $R_n A$ at low temperature for YBCO at 4.2 K²⁰, NdFeAs(O,F) at 4.2 K⁹², Ba(Fe_{1-x}Co_x)₂As₂ (Co-doped Ba-122 at 4 K⁹⁸), BaFe₂(As_{1-x}P_x)₂ (P-doped Ba-122 at 2 K¹⁰¹), and Fe(Se,Te) at 4.2 K^{104,105}.

ACKNOWLEDGMENTS

This work was supported by the JSPS Grant-in-Aid for Scientific Research (B) Grant Number 16H04646 as well as JST CREST Grant Number JPMJCR18J4.

REFERENCES

- ¹Tomimoto K, Terasaki I, Rykov A I, Miura T and Tajima S, 1999 *Phys. Rev. B* **60** 114
- ²Tsuei C C and Kirtley J R 2000 *Rev. Mod. Phys.* **72** 969
- ³Hilgenkamp H and Mannhart J 2002 *Rev. Mod. Phys.* **74** 485
- ⁴Putti M, Pallecchi I, Bellingeri E, Cimberle M R, Tropeano M, Ferdeghini C, Palenzona A, Tarantini C, Yamamoto A, Jiang J, Jaroszynski J, Kametani F, Abraimov D, Polyanskii A, Weiss J D, Hellstrom E E, Gurevich A, Larbalestier D C, Jin R, Sales B C, Sefat A S, McGuire M A, Mandrus D, Cheng P, Jia Y, Wen H H, Lee S and Eom C B, 2010 *Supercond. Sci. Technol.* **23** 034003
- ⁵Chan Siu-Wai 1994 *J. Phys. Chem. Solids* **55** 1415
- ⁶Durrell J H and Rutter N A 2009 *Supercond. Sci. Technol.* **22** 013001
- ⁷Durrell J H, Eom C-B, Gurevich A, Hellstrom E E, Tarantini C, Yamamoto A and Larbalestier D C 2011 *Rep. Prog. Phys.* **74** 124511
- ⁸Hänisch J and Iida K, *Superconductivity From Materials Science to Practical Applications* (Springer), Chap. 10, pp. 269-302.
- ⁹Seuntjens J M and Larbalestier D C 1990 *J. Appl. Phys.* **67** 2007
- ¹⁰Holzappel B, Verebelyi D, Cantoni C, Paranthaman M, Sales B, Feenstra R, Christen D and Norton D P 2000 *Physica C* **341-348** 1431
- ¹¹Schoop U, Kleefisch S, Meyer S, Marx A, Alff L, Gross R, Naito M and Sato H 1999 *IEEE. Trans. Appl. Supercond.* **9** 3409
- ¹²Hänisch J, Attenberger A, Holzappel B and Schultz L 2002 *Phys. Rev. B* **65** 052507

- ¹³Gurevich A and Pashitskii E A 1998 *Phys. Rev. B* **57** 13878
- ¹⁴Song X, Daniels G, Feldmann D M, Gurevich A and Larbalestier D 2005 *Nat. Mater.* **4** 470
- ¹⁵Deutscher G 2010 *Appl. Phys. Lett.* **96** 122502
- ¹⁶Mannhart J and Hilgenkamp H 1997 *Supercond. Sci. Technol.* **10** 880
- ¹⁷Kasatkin A, Tsvetkovskii V and Borisenko P 2013 *Universal Journal of Physics and Application* **1** 144
- ¹⁸Graser S, Hirschfeld P J, Kopp T, Guster R, Andersen B M and Mannhart J 2010 *Nat. Phys.* **6** 609
- ¹⁹Schmehl A, Goetz B, Schulz R R, Schneider C W, Bielefeldt H, Hilgenkamp H and Mannhart J 1999 *EPL* **47** 110
- ²⁰Hilgenkamp H and Mannhart J 1998 *Appl. Phys. Lett.* **73** 265
- ²¹Daniels G A, Gurevich A and Larbalestier D C 2000 *Appl. Phys. Lett.* **77** 3251
- ²²Díaz A, Mechin L, Berghuis P and Evetts J E 1998 *Phys. Rev. B* **58** R2960
- ²³Hammerl G, Schmehl A, Schulz R R, Goetz B, Bielefeldt H, Schneider C W, Hilgenkamp H and Mannhart J 2000 *Nature* **407** 162
- ²⁴Fâte A and Senatore C 2018 *Sci. Rep.* **8** 17703
- ²⁵Yuan H, Shimotani H, Tsukazaki A, Ohtomo A, Kawasaki M and Iwasa Y 2009 *Adv. Funct. Mater.* **19** 1046
- ²⁶Hassan M U and Wimbush S C 2015 *Phys. Status Solidi A* **212** 2037
- ²⁷Jin S, Tiefel T H, Sherwood R C, Kammlott G W and Zahurak S M 1987 *Appl. Phys. Lett.* **51** 943
- ²⁸Sawano K, Morita M, Tanaka M, Sasaki T, Kimura K, Takebayashi S, Kimura M and Miyamoto K 1991 *Jpn. J. Appl. Phys.* **30** L1157
- ²⁹Durrell J H, Dennis A R, Jaroszynski J, Ainslie M D, Palmer K G B, Shi Y-H, Campbell A M, Hull J, Strasik M, Hellstrom E E and Cardwell D A 2014 *Supercond. Sci. Technol.* **27** 082001
- ³⁰Patel A, Baskys A, Mitchell-Williams T, McCaul A, Coniglio W, Hänisch J,

- Lao M and Glowacki B A 2018 *Supercond. Sci. Technol.* **31** 09LT01
- ³¹Durrell J H, Ainslie M D, Zhou D, Vanderbemden P, Bradshaw T, Speller S, Filipenko M and Cardwell D A 2018 *Supercond. Sci. Technol.* **31** 103501
- ³²Dam B, Huijbregtse J M, Klaassen F C, van der Geest R C F, Doornbos G, Rector J H, Testa A M, Freisem S, Martinez J C, Stäuble-Pümpin B and Griessen R 1999 *Nature* **399** 439
- ³³Iijima Y, Tanabe N, Ikeno Y and Kohno O 1991 *Physica C* **185-189** 1959
- ³⁴Goyal A, Norton D P, Budai J D, Paranthaman M, Specht E D, Kroeger D M, Christen D K, He Q, Saffian B, List F A, Lee D F, Martin P M, Klabunde C E, Hartfield E and Sikka V K 1996 *Appl. Phys. Lett.* **69** 1795
- ³⁵Buzea C and Yamashita T 2001 *Supercond. Sci. Technol.* **14** R115
- ³⁶Larbalestier D C, Cooley L D, Rikel M O, Polyanskii A A, Jiang J, Patnaik S, Cai X Y, Feldmann D M, Gurevichi A, Squitieri A A, Naus M T, Eom C B, Hellstrom E E, Cava R J, Regan K A, Rogado N, Hayward M A, He T, Slusky J S, Khalifah P, Inumaru K and Haas M 2001 *Nature* **410** 186
- ³⁷Dhallé M, Toulemonde P, Beneduce C, Musolino N, Decroux M and Flükiger R 2001 *Physica C* **363** 155
- ³⁸Glowacki B A, Majoros M, Vickers M, Evetts J E, Shi Y and Mcdougall I 2001 *Supercond. Sci. Technol.* **14** 193
- ³⁹Grasso G, Malagoli A, Ferdeghini C, Roncallo S, Braccini V, Siri A S and Cimberle M R 2001 *Appl. Phys. Lett.* **79** 230
- ⁴⁰Kumakura H, Matsumoto A, Fujii H and Togano K 2001 *Appl. Phys. Lett.* **79** 2435
- ⁴¹Kitaguchi H, Matsumoto A, Kumakura H, Doi T, Yamamoto H, Saitoh K, Sosiati H and Hata S 2004 *Appl. Phys. Lett.* **85** 2842
- ⁴²Martínez E, Mikheenko P, Martínez-López M, Millán A, Bevan A and Abell J S 2007 *Phys. Rev. B* **75** 134515
- ⁴³Collings E W, Sumption M D, Bhatia M, Susner M A and Bohnenstiehl S D

- 2008 *Supercond. Sci. Technol.* **21** 103001
- ⁴⁴Matsushita T, Kiuchi M, Yamamoto A, Shimoyama J-I and Kishio K 2008 *Supercond. Sci. Technol.* **21** 015008
- ⁴⁵Senkowicz B J, Mungall R J, Zhu Y, Jiang J, Voyles P M, Hellstrom E E and Larbalestier D C 2008 *Supercond. Sci. Technol.* **21** 035009
- ⁴⁶Rosová A, Hušek I, Kulich M, Melišek T, Kováč P, Dobročka E, Kopera L, Scheiter J and Häßler W 2018 *J. Alloys Compd.* **764** 437
- ⁴⁷Malagoli A, Braccini V, Tropeano M, Vignolo M, Bernini C, Fanciulli C, Romano G, Putti M, Ferdeghini C, Mossang E, Polyanskii A and Larbalestier D C 2008 *J. Appl. Phys.* **104** 103908
- ⁴⁸Fujii H, Iwanade A, Kawada S and Kitaguchi H 2018 *Cryogenics* **89** 76
- ⁴⁹Fujii H, Iwanade A and Kitaguchi H 2019 *Physica C* **559** 32
- ⁵⁰Sugino S, Yamamoto A, Shimoyama J-I and Kishio K 2015 *Supercond. Sci. Technol.* **28** 055016
- ⁵¹Yamamoto A, Shimoyama J-I, Ueda S, Katsura Y, Horii S and Kishio K 2005 *Supercond. Sci. Technol.* **18** 116
- ⁵²Kim J H, Dou S X, Wang J L, Shi D Q, Xu X, Hossain M S A, Yeoh W K, Choi S and Kiyoshi T 2007 *Supercond. Sci. Technol.* **20** 448
- ⁵³Cai Q, Liu Y C, Ma Z Q, Yu L M and Li H J 2017 *J. Mater. Sci.: Mater.* **28** 5645
- ⁵⁴Cai Q, Liu Y C, Xiong J and Ma Z Q 2018 *J. Mater. Sci.: Mater.* **29** 10323
- ⁵⁵Qaid S A S, Alzayed N S, Shahabuddin M, Ramay S M and Atiq S 2017 *J. Mater. Sci.: Mater.* **28** 14696
- ⁵⁶Zhao Q, Jiao C J, Zhu E L and Zhu Z 2017 *J. Alloys Compd.* **717** 19
- ⁵⁷Cheng F, Ma Z Q, Liu C X, Li H J, Hossain M A, Bando Y, Yamaguchi Y, Fatehmulla A, Farooq W A and Liu Y C 2017 *J. Alloys Compd.* **727** 1105
- ⁵⁸Ma Z Q, Liu Y C, Shi Q Z, Zhao Q and Gao Z M 2008 *Supercond. Sci. Technol.* **21** 065004

- ⁵⁹Ma Z Q, Liu Y C, Shi Q Z, Zhao Q and Gao Z M 2009 *Mater. Res. Bull.* **44** 531
- ⁶⁰Ma Z Q, Liu Y C and Gao Z M 2010 *Scr. Mater.* **63** 399
- ⁶¹Shimoyama J, Hanafusa K, Yamamoto A, Katsura Y, Horii S, Kishio K and Kumakura H 2007 *Supercond. Sci. Technol.* **20** 307
- ⁶²Ozturk K, Dancer C E J, Savaskan B, Aksoy C, Guner B, Badica P, Aldica G and Celik S 2017 *J. Alloys Compd.* **724** 427
- ⁶³Tachikawa K, Yamada Y, Suzuki O, Enomoto M and Aodai M 2002 *Physica C* **382** 108
- ⁶⁴Takahashi Y, Naito T and Fujishiro H 2017 *Supercond. Sci. Technol.* **30** 125006
- ⁶⁵Durrell J H, Dancer C E J, Dennis A, Shi Y, Xu Z, Campbell A M, Babu N H, Todd R I, Grovenor C R M and Cardwell D A 2012 *Supercond. Sci. Technol.* **25** 112002
- ⁶⁶Fuchs G, Häbler, Nenkov K, Scheiter J, Perner O, Handstein A, Kanai T, Schultz L and Holzapfel B 2013 *Supercond. Sci. Technol.* **26** 122002
- ⁶⁷Prikhna T A, Eisterer M, Rindfleisch M, Ortino M, Kozyrev A V, Shaternik A V, Shaternik V E, Tomsic M, Moshchil V E, Karpets M V, Sverdun V B, Ponomaryov S S, Romaka V V and Seidel P 2019 *IEEE. Trans. Appl. Supercond.* **29** 6200905
- ⁶⁸Yamada Y, Ohuchi H, Yamamoto A and Kishio K 2016 *J. Japan Inst. Met. Mater.* **80** 457
- ⁶⁹Aldica G, Burdusel M, Popa S, Enculescu M, Pasuk I and Badica P 2015 *Physica C* **519** 184
- ⁷⁰Badica P, Burdusel M, Popa S, Pasuk I, Ivan I, Borodianska H, Vasylykiv O, Kuncser A, Ionescu A M, Miu L and Aldica G 2016 *Supercond. Sci. Technol.* **29** 105020
- ⁷¹Badica P, Batalu D, Burdusel M, Grigoroscuta M A, Aldica G V, Enculescu M, Gabor R A, Wang Z Y, Huang R X and Li P F 2018 *Ceram. Int.* **44** 10181

- ⁷²Berger K, Koblishka M R, Douine B, Noudem J, Bernstein P, Hauet T and Lévêque J 2016 *IEEE. Trans. Appl. Supercond.* **26** 6801005
- ⁷³Murakami A, Iwamoto A and Noudem J G 2018 *IEEE. Trans. Appl. Supercond.* **28** 8400204
- ⁷⁴Häßler W, Scheiter J, Hädrich P, Kauffmann-Weiss S, Holzapfel B, Oomen M and Nielsch K 2018 *Physica C* **551** 48
- ⁷⁵Giunchi G, Ripamonti G, Perini E, Cavallin T and Bassani E 2007 *IEEE. Trans. Appl. Supercond.* **17** 2761
- ⁷⁶Giunchi G 2011 *IEEE. Trans. Appl. Supercond.* **21** 1564
- ⁷⁷Ueda S, Shimoyama J-I, Iwayama I, Yamamoto A, Katsura Y, Horii S and Kishio K 2005 *Appl. Phys. Lett.* **86** 222502
- ⁷⁸Togano K, Hur J M, Matsumoto A and Kumakura H 2009 *Supercond. Sci. Technol.* **22** 015003
- ⁷⁹Li G Z, Sumption M D, Susner M A, Yang Y, Reddy K M, Rindfleisch M A, Tomsic M J, Thong C J and Collings E W 2012 *Supercond. Sci. Technol.* **25** 115023
- ⁸⁰Bhagurkar A G, Yamamoto A, Anguilano L, Dennis A R, Durrell J H, Babu N H and Cardwell D A 2016 *Supercond. Sci. Technol.* **29** 035008
- ⁸¹Bhagurkar A G, Yamamoto A, Dennis A R, Durrell J H, Aljohani T A, Babu N H and Cardwell D A 2017 *J. Am. Ceram. Soc.* **100** 2451
- ⁸²Bhagurkar A G, Yamamoto A, Wang L, Xia M, Dennis A R, Durrell J H, Aljohani T A, Babu N H and Cardwell D A 2018 *Sci. Rep.* **8** 13320
- ⁸³Gozzelino L, Gerbaldo R, Ghigo G, Laviano F, Torsello D, Bonino V, Truccato M, Batalu D, Grigoroscuta M A, Burdusel M, Aldica G V and Badica P 2019 *Supercond. Sci. Technol.* **32** 034004
- ⁸⁴Savaşkan B, Koparan E T, Güner S B, Öztürk K and Çelik Ş 2019 *J. Supercond. Magn.* **32** 827
- ⁸⁵Yamamoto A, Jiang J, Tarantini C, Craig N, Polyanskii A A, Kametani F,

- Hunte F, Jaroszynski J, Hellstrom E E, Larbalestier D C, Jin R, Sefat A S, McGuire M A, Sales B C, Christen D K and Mandrus D 2008 *Appl. Phys. Lett.* **92** 252501
- ⁸⁶Haindl S, Kidszun M, Kauffmann A, Nenkov K, Kozlova N, Freudenberger J, Thersleff T, Hänisch J, Werner J, Reich E, Schultz L and Holzapfel B *Phys. Rev. Lett.* **104** 077001
- ⁸⁷Kametani F, Polyanskii A A, Yamamoto A, Jiang J, Hellstrom E E, Gurevich A, Larbalestier D C, Ren Z A, Yang J, Dong X L, Lu W and Zhao Z X 2008 *Supercond. Sci. Technol.* **22** 015010
- ⁸⁸Senatore C, Flükiger R, Cantoni M, Wu G, Liu R H and Chen X H 2008 *Phys. Rev. B* **78** 054514
- ⁸⁹Yamamoto A, Polyanskii A A, Jiang J, Kametani F, Tarantini C, Hunte F, Jaroszynski J, Hellstrom E E, Lee P J, Gurevich A, Larbalestier D C, Ren Z A, Yang J, Dong X L, Lu W and Zhao Z X 2008 *Supercond. Sci. Technol.* **21** 095008
- ⁹⁰Omura T, Matsumoto T, Hatano T, Iida K and Ikuta H 2018 *J. Phys.: Conf. Ser.* **1054** 012024
- ⁹¹Kawaguchi T, Uemura H, Ohno T, Tabuchi M, Ujihara T, Takeda Y and Ikuta H 2011 *Appl. Phys. Express* **4** 083102
- ⁹²Iida K, Omura T, Matsumoto T, Hatano T and Ikuta H 2019 *Supercond. Sci. Technol.* **32** 074003
- ⁹³Katase T, Hiramatsu H, Matias V, Sheehan C, Ishimaru Y, Kamiya T, Tanabe K and Hosono H 2011 *Appl. Phys. Lett.* **98** 242510
- ⁹⁴Sato H, Hiramatsu H, Kamiya T and Hosono H 2016 *Sci. Rep.* **6** 36828
- ⁹⁵Corrales-Mendoza I, Labias-Romero J, Castillo N and Conde-Gallardo A 2019 *Supercond. Sci. Technol.* **32** 055005
- ⁹⁶Matsumoto J, Hanzawa K, Sasase M, Haindl S, Katase T, Hiramatsu H and Hosono H 2019 *Phys. Rev. Materials* **3** 103401

- ⁹⁷Lee S, Jiang J, Weiss J D, Folkman C M, Bark C W, Tarantini C, Xu A, Abraimov D, Polyanski A, Nelson C T, Zhang Y, Baek S H, Jang H W, Yamamoto A, Kametani F, Pan X Q, Hellstrom E E, Gurevich A, Eom C B and Larbalestier D C 2009 *Appl. Phys. Lett.* **95** 212505
- ⁹⁸Katase T, Ishimaru Y, Tsukamoto A, Hiramatsu H, Kamiya T, Tanabe K and Hosono H 2011 *Nat. Commun.* **2** 409
- ⁹⁹Hiramatsu H, Katase T, Ishimaru Y, Tsukamoto A, Kamiya T, Tanabe K and Hosono H 2012 *Mater. Sci. Eng., B* **177** 515
- ¹⁰⁰Iida K, Haindl S, Kurth F, Hänisch J, Schultz L and Holzapfel B 2013 *Physics Procedia* **45** 189
- ¹⁰¹Sakagami A, Kawaguchi T, Tabuchi M, Ujihara T, Takeda Y and Ikuta H 2013 *Physica C* **494** 181
- ¹⁰²Eisterer M 2019 *Phys. Rev. B* **99** 094501
- ¹⁰³Hänisch J, Iida K, Kurth F, Thersleff T, Trommler S, Reich E, Hühne R, Schultz L and Holzapfel B 2014 *AIP Conference Proceedings* **1574** 260
- ¹⁰⁴Sarnelli E, Adamo M, Nappi C, Braccini V, Kawale S, Bellingeri E and Ferdeghini C 2014 *Appl. Phys. Lett.* **104** 162601
- ¹⁰⁵Si W, Zhang C, Shi X, Ozaki T, Jaroszynski J and Li Q 2015 *Appl. Phys. Lett.* **106** 032602
- ¹⁰⁶Sarnelli E, Nappi C, Camerlingo C, Enrico E, Bellingeri E, Kawale S, Braccini V, Leveratto A and Ferdeghini C 2017 *IEEE. Trans. Appl. Supercond.* **27** 7400104
- ¹⁰⁷Gross P, Chaudhari P, Dimos D, Gupta A and Kogan G 1990 *Phys. Rev. Lett.* **64** 228
- ¹⁰⁸Iida K, Kurth F, Chihara M, Sumiya N, Grinenko V, Ichinose A, Tsukada I, Hänisch J, Matias V, Hatano T, Holzapfel B and Ikuta H 2014 *Appl. Phys. Lett.* **105** 172602
- ¹⁰⁹Zhang Q, Zhang X, Yao C, Huang H, Wang D, Dong C, Ma Y, Ogino H and Awaji S 2017 *Supercond. Sci. Technol.* **30** 065004

- ¹¹⁰Tarantini C, Iida K, Hänisch J, Kurth F, Jaroszynski J, Sumiya N, Chihara M, Hatano T, Ikuta H, Schmidt S, Seidel P, Holzapfel B and Larbalestier D C 2016 *Sci. Rep.* **6** 36047
- ¹¹¹Guo Z, Saito H, Kondo K, Matsumoto T, Hatano T, Iida K, Hänisch J, Ikuta H and Hata S, in preparation
- ¹¹²Iida K, Hänisch J, Trommler S, Matias V, Haindl S, Lucas del Pozo I, Hühne R, Kieszun M, Engelmann J, Schultz L and Holzapfel B 2011 *Appl. Phys. Express* **4** 013103
- ¹¹³Trommler S, Hänisch J, Matias V, Hühne R, Reich E, Iida K, Haindl S, Schultz L and Holzapfel B 2012 *Supercond. Sci. Technol.* **25** 084019
- ¹¹⁴Xu Z, Yuan P, Fan F and Ma Y 2018 *Supercond. Sci. Technol.* **31** 055001
- ¹¹⁵Gurevich A, Rzechowski M S, Daniels G, Patnaik S, Hinaus B M, Carillo F, Tafuri F and Larbalestier D C 2002 *Phys. Rev. Lett.* **88** 097001
- ¹¹⁶Horide T, Matsumoto K, Ichinose A, Mukaida M, Yoshida Y and Horii S 2007 *Phys. Rev. B* **75** 020504
- ¹¹⁷Palau A, Puig T, Obradors X, Feenstra R and Gapud A A 2006 *Appl. Phys. Lett.* **88** 122502
- ¹¹⁸Iida K, Sato H, Tarantini C, Hänisch J, Jaroszynski J, Hiramatsu H, Holzapfel B and Hosono H 2017 *Sci. Rep.* **7** 39951
- ¹¹⁹Rodríguez O and Mariño A 2015 *Physica C* **513** 9
- ¹²⁰Kametani F, Li P, Abraimov D, Polyanskii A A, Yamamoto A, Jiang J, Hellstrom E E, Gurevich A, Larbalestier D C, Ren Z A, Yang J, Dong X L, Lu W and Zhao Z X 2009 *Appl. Phys. Lett.* **95** 142502
- ¹²¹Hosono H, Tanabe K, Takayama-Muromachi E, Kageyama H, Yamanaka S, Kumakura H, Nohara M, Hiramatsu H and Fujitsu S 2015 *Sci. Technol. Adv. Mater.* **16** 033503
- ¹²²Si W, Zhou J, Jie Q, Dimitrov I, Solovyov V, Johnson P D, Jaroszynski J, Matias V, Sheehan C and Li Q 2011 *Appl. Phys. Lett.* **98** 262509

- ¹²³Xu Z, Yuan P, Ma Y and Cai C 2017 *Supercond. Sci. Technol.* **30** 035003
- ¹²⁴Si W, Han S, Shi X, Ehrlich S N, Jaroszynski J, Goyal A and Li Q 2013 *Nat. Commun.* **4** 1347
- ¹²⁵Sylva G, Augieri A, Mancini A, Rufoloni A, Vannozzi A, Celentano G, Bellingeri E, Ferdeghini C, Putti M and Braccini V 2019 *Supercond. Sci. Technol.* **32** 084006
- ¹²⁶Hosono H, Yamamoto A, Hiramatsu H and Ma Y 2018 *Materials Today* **21** 278
- ¹²⁷Yao C and Ma Y W 2019 *Supercond. Sci. Technol.* **32** 023002
- ¹²⁸Weiss J D, Tarantini C, Jiang J, Kametani F, Polyanskii A A, Larbalestier D C and Hellstrom E E 2012 *Nat. Mater.* **11** 682
- ¹²⁹Zhang X P, Yao C, Lin H, Cai Y, Chen Z, Li J Q, Dong C H, Zhang Q J, Wang D L, Ma Y W, Oguro H, Awaji S and Watanabe K 2014 *Appl. Phys. Lett.* **104** 202601
- ¹³⁰Gao Z S, Togano K, Matsumoto A and Kumakura H 2014 *Sci. Rep.* **4** 4065
- ¹³¹Wang D L, Zhang Z, Zhang X P, Jiang D H, Dong C H, Huang H, Chen W G, Xu Q J and Ma Y W 2019 *Supercond. Sci. Technol.* **32** 04LT01
- ¹³²Weiss J D, Yamamoto A, Polyanskii A A, Richardson R B, Larbalestier D C and Hellstrom E E 2015 *Supercond. Sci. Technol.* **28** 112001
- ¹³³Iida K 2015 *Supercond. Sci. Technol.* **28** 120501
- ¹³⁴Ainslie M D, Yamamoto A, Fujishiro H, Weiss J D, Hellstrom E E 2017 *Supercond. Sci. Technol.* **30** 105009
- ¹³⁵Pyon S, Suwa T, Tamegai T, Takano K, Kajitani H, Koizumi N, Awaji S, Zhou N and Shi Z X 2018 *Supercond. Sci. Technol.* **31** 055016
- ¹³⁶Pyon S, Tsuchiya Y, Inoue H, Koizumi N, Kajitani H and Tamegai T 2014 *Physica C* **504** 69
- ¹³⁷Tamegai T, Pyon S, Tsuchiya Y, Inoue H, Koizumi N and Kajitani H 2015 *IEEE. Trans. Appl. Supercond.* **25** 7300504
- ¹³⁸Togano K, Gao Z, Matsumoto A and Kumakura H 2013 *Supercond. Sci. Technol.*

26 115007

- ¹³⁹Huang H, Yao C, Dong C H, Zhang X P, Wang D L, Cheng Z, Li J Q, Awaji S, Wen H H and Ma Y W 2018 *Supercond. Sci. Technol.* **31** 015017
- ¹⁴⁰Liu S F, Cheng Z, Yao C, Dong C H, Wang D L, Huang H, Li L, Xu G X, Zhu Y C, Liu F, Liu H J and Ma Y W 2019 *Supercond. Sci. Technol.* **32** 044007
- ¹⁴¹Xu G X, Zhang X P, Yao C, Huang H, Zhu Y C, Li L, Cheng Z, Liu S F, Huang S Y and Ma Y W 2019 *Physica C* **561** 30
- ¹⁴²Togano K, Gao Z, Matsumoto A, Kikuchi A and Kumakura H 2017 *Supercond. Sci. Technol.* **30** 015012
- ¹⁴³Weiss J D, Jiang J, Polyanskii A A and Hellstrom E E 2013 *Supercond. Sci. Technol.* **26** 074003
- ¹⁴⁴Tokuta S and Yamamoto A 2019 *APL Mater.* **7** 111107
- ¹⁴⁵Hecher J, Baumgartner T, Weiss J D, Tarantini C, Yamamoto A, Jiang J, Hellstrom E E, Larbalestier D C and Eisterer M 2016 *Supercond. Sci. Technol.* **29** 025004
- ¹⁴⁶Shimada Y, Yamamoto A, Hayashi Y, Kishio K, Shimoyama J-I, Hata S and Konno T J 2019 *Supercond. Sci. Technol.* **32** 084003
- ¹⁴⁷Kim Y-J, Weiss J D, Hellstrom E E, Larbalestier D C and Seidman D N 2014 *Appl. Phys. Lett.* **105** 162604
- ¹⁴⁸Winkler D, Zhang Y M, Nilsson P Å, Stepantsov E A and Claeson T 1994 *Phys. Rev. Lett.* **72** 1260
- ¹⁴⁹Hong S-H, Lee N, Kang W and Lee S-G 2014 *Supercond. Sci. Technol.* **27** 055007
- ¹⁵⁰Qin D, Iida K, Naito M and Yamamoto A 2019 Growth of Thin Films of $\text{Ba}_{1-x}\text{K}_x\text{Fe}_2\text{As}_2$ by MBE *The 80th JSAP Autumn Meeting* <https://confit.atlas.jp/guide/event/jsap2019a/subject/19p-C213-14/advanced>